

Received 20xx month day; accepted 20xx month day

Key words: stars: early-type – methods: data analysis – techniques: photometric – astronomical databases: catalogs

Discovery of 2716 hot emission-line stars from LAMOST DR5

B. Shridharan¹, Blesson Mathew¹, S. Nidhi¹, R. Anusha¹, R. Arun¹, Sreeja S. Kartha¹ and Yerra Bharat Kumar²

¹ Department of Physics and Electronics, CHRIST (Deemed to be University), Bangalore 560029, India; shridharan.b@res.christuniversity.in

² Key Laboratory of Optical Astronomy, National Astronomical Observatories, Chinese Academy of Sciences, Beijing 100101, China

Abstract We present a catalog of 3339 hot emission-line stars (ELS) identified from 451,695 O, B, and A type spectra, provided by the LAMOST DR5 release. We developed an automated python routine that identified 5437 spectra having a peak between 6561 and 6568 Å. False detections and bad spectra were removed, leaving 4138 good emission-line spectra of 3339 unique ELS. We re-estimated the spectral type of 3307 spectra as the LAMOST Stellar Parameter Pipeline (LASP) did not provide accurate spectral types for these emission-line spectra. As Herbig Ae/Be stars show higher excess in near-infrared and mid-infrared wavelengths than Classical Ae/Be stars, we used 2MASS and WISE photometry to distinguish them. Finally, we report 1089 Classical Be, 233 Classical Ae, and 56 Herbig Ae/Be stars identified from the LAMOST DR5. In addition, 928 B[em]/A[em] stars and 240 CAe/CBe potential candidates are identified. From our sample of 3339 hot emission-line stars, 2716 ELS identified in this work do not have any record in the SIMBAD database and they can be considered as new detections. Identification of such a large homogeneous set of emission-line spectra will help the community to study the emission phenomenon in detail without worrying about the inherent biases when compiling from various sources.

1 INTRODUCTION

Stars with bright emission lines in the spectrum indicating unusual activities in the stellar atmosphere has become a subject of much astrophysical research. Objects with such diverse spectra showing Balmer emission along with metallic emission lines are generally known as Emission-line stars (ELS). These lines arising from the circumstellar disk/envelope of the star are formed due to the recombination process. Based on the evolutionary stage, spectral type, and mass, ELS can be classified into various categories such as Young Stellar Objects (YSOs), Oe/Be/Ae stars, Wolf-Rayet (WR) stars, Supergiants, Planetary Nebulae (PNe), Luminous Blue Variables (LBVs), Mira stars, Flare stars, and Symbiotic stars (Kogure & Leung 2007). Hence, the study of ELS can provide insight towards the line formation regions and various evolutionary phases of stars.

In recent years, research on ELS (Vioque et al. 2020; Akras et al. 2019; Huang et al. 2013) has surged due to the availability of photometric surveys (*Gaia*, 2MASS, IPHAS, etc.) and large scale spectroscopic surveys (LAMOST, SDSS, APOGEE). Merrill & Burwell (1949) were the first to undertake a survey on ELS in which spectra of early-type stars with bright hydrogen lines were detected. Wackerling (1970) compiled a catalogue of 5,326 early-type ELS in our Galaxy. Later, Allen (1973) observed nearly 250 early-type ELS in the near-infrared (NIR) wavelengths and proposed a mechanism wherein the excess flux in NIR (IR excess) arises due to the thermal radiation from the dust in the circumstellar disk and the electron *bremstrahlung* originating from a shell of ionized gas. Following these works, Stephenson & Sanduleak (1977) identified 455 new bright H α stars in our galaxy using objective-prism plates. By the end of 20th century, various surveys increased the count of ELS considerably. One of the most extensive ELS survey in H α regime was performed by Kohoutek & Wehmeyer (1999), in which they provided a catalog of 4174 H α ELS in the Northern Milky Way within the latitude range of $-10^\circ < b < 10^\circ$. Following Kohoutek & Wehmeyer (1999), a much larger and deeper survey was performed and is now known as, The INT Photometric H α Survey of the Northern Galactic Plane (IPHAS; Drew et al. 2005). It covered the Milky Way in H α , Sloan r' and i' bands within a magnitude range of $13 \leq r' \leq 19.5$ mag. Following the initial data release from IPHAS (González-Solares et al. 2008), a series of studies on different types of ELS

were published. [Witham et al. \(2008\)](#) presented the preliminary catalogue of 4853 $H\alpha$ emission sources from IPHAS. Various ELS classes including cataclysmic variables ([Witham et al. 2007](#)), symbiotic stars ([Corradi et al. 2008, 2010](#); [Rodríguez-Flores et al. 2014](#)), YSOs ([Vink et al. 2008](#); [Barentsen et al. 2011](#)) and classical Be stars ([Raddi et al. 2013](#)) were identified from the survey. Similarly, [Kalari et al. \(2015\)](#) has studied the accretion rates of 235 Classical T Tauri star (CTTs) candidates in the Lagoon Nebula using the VST Photometric $H\alpha$ Survey of the Southern Galactic Plane and Bulge (VPHAS+; [Drew et al. 2014](#)). There are quite a few studies which searched for ELS in open clusters. For example, [Mathew et al. \(2008\)](#) identified 157 ELS from the slitless spectroscopic survey of 207 open clusters in the Galaxy. [Reipurth et al. \(2004\)](#) and [Pettersson et al. \(2014\)](#) presented $H\alpha$ ELS surveys in various molecular clouds using the wide field-objective prism films. Recently, [Vioque et al. \(2020\)](#) identified new ELS candidates using machine learning techniques on data from *Gaia* DR2, 2MASS, WISE and IPHAS or VPHAS+ surveys.

The Large Sky Area Multi-Object fiber Spectroscopic Telescope (LAMOST) surveys have accumulated millions of spectra over a period of 5-6 years. Even though a huge spectral database from LAMOST is made available to the public, very few works have identified and characterized ELS spectra till date. [Lin et al. \(2015\)](#) identified 192 Classical Be (CBe) star candidates from LAMOST DR1, which increased the then known sample of CBe stars by about 8%. Similarly, a study on ELS and $H\alpha$ line profiles from LAMOST DR2 were conducted by [Hou et al. \(2016\)](#), in which 10,436 early-type ELS were identified. [Yao et al. \(2017\)](#) have studied Mira Variable Stars identified from LAMOST DR4 and [Li et al. \(2018\)](#) identified 6 new Oe stars from LAMOST DR5.

In this work, we make use of the extensive data available to us from LAMOST DR5 release to identify early-type ELS and mainly classify them into CBe stars and Herbig Ae/Be stars (HAeBe). A CBe star is a fast rotating B-type non-super giant with an equatorial decretion disk ([Porter & Rivinius 2003](#)). The disk is transient in nature identified through the change in $H\alpha$ emission strength over a timescale of years to decades ([Štefl et al. 2003](#)). The formation of decretion disk in CBe stars is known as ‘Be phenomenon’. The episodic occurrence of mass loss which results in the formation of a decretion disk is still an open question. The emission strength of $H\alpha$ and other hydrogen and metallic emission lines were analyzed to understand the ‘Be phenomenon’ in CBe stars ([Rivinius et al. 2013](#), for a review). Most CBe stars span the spectral range of B0 - B9, even though a few late O ([Li et al. 2018](#)) and early A type stars ([Jaschek et al. 1986](#); [Anusha et al. 2021](#)) are included in this class. Also, CBe stars are defined to belong in the luminosity class III to V ([Jaschek & Egret 1982](#)). In contrast to CBe stars, pre-main sequence (PMS) stars are very young objects that have not started hydrogen burning. The low-mass (0.1 to 2 M_{\odot}) PMS stars are known as T Tauri stars ([Joy 1945](#)), whereas those in the intermediate-mass range (2 to 8 M_{\odot}) are called HAeBe stars ([Herbig 1960](#); [Waters & Waelkens 1998](#)). HAeBe and T Tauri stars share common characteristics such as the circumstellar accretion disk, IR excess, Balmer emission lines and metallic emission lines ([Hillenbrand et al. 1992](#)). For the present study, we discuss the ELS belonging to O, B and A spectral types, whereas those belonging to later spectral types will be discussed in a follow-up study (Edwin et al. in prep).

We downloaded spectra of O, B, and A type stars from LAMOST DR5 and developed a python routine to identify spectra with $H\alpha$ in emission. To re-estimate the spectral types of ELS spectra, we performed a visually aided semi-automated template matching process using MILES spectral library. Further, we made use of available photometric data from missions/surveys such as 2MASS, WISE, *Gaia* EDR3 and APASS to sub-classify our sample into CBe stars and HAeBe stars. We categorized the identified ELS spectra into various classes, as explained in subsection 3.5.

The structure of the paper is as follows. Section 2 provides a brief introduction of the LAMOST survey and explains the data collection along with the spectra normalization procedure. In Section 3, we discuss the ELS identification and classification procedure along with the explanation of spectral-type re-estimation technique. We have also detailed the naming convention employed in this work. In Section 4, we plot infrared color-color diagram (CCDm) and *Gaia* color-magnitude diagram (CMD), followed by discussion of spectral features seen in different classes identified in this work. We cross-matched our list with the SIMBAD database to verify our classifications. The major results of our work are summarized in Section 5. Description of our catalog is given in Appendix A, automated forbidden line identification criteria is given in Appendix B and necessary information for a representative sample of ELS identified are given in Appendix C.

2 DATA COLLECTION

2.1 About LAMOST Data Release 5

The LAMOST is a reflecting Schmidt telescope, with an effective aperture of 3.6 m - 4.9 m and a wide Field of View (FoV) of 5° ([Cui et al. 2012](#); [Wang et al. 1996](#)). It is also known as Guo Shoujing Telescope, maintained by Xinglong station of the National Astronomical Observatories, Chinese Academy of Sciences. It is equipped with 4000 optical fibers in its focal plane with 16 low-resolution spectrographs and 32 Charge-Coupled Devices (CCD) ([Zhao et al. 2012](#)). It is designed with three major components: the correcting mirror *Ma*, the primary mirror *Mb* and a focal surface ([Cui et al. 2012](#)). Objects with *r*-band magnitude up to ~ 20 mag are observed by LAMOST in the wavelength range of 3690 – 9000 Å with spectral resolution of $R \sim 1800$ ([Cui et al. 2012](#)). The Galactic and

Extra Galactic surveys conducted by LAMOST are classified into two major projects: LAMOST Experiment for Galactic Understanding and Exploration (LEGUE; Deng et al. 2012) and LAMOST Extra Galactic Survey (LEGAS; Zhao et al. 2012).

2.2 Data Collection and Spectral Normalization

During the five-year regular survey, the raw data was reduced by LAMOST two-dimensional (2D) pipeline (Luo et al. 2015), which used procedures similar to those of SDSS spectro2d pipeline (Stoughton et al. 2002). A spectrum of a light beam from fiber is imaged onto the 32 cameras using $4k \times 4k$ CCD chips (Wei & Stover 1996). The data from each CCD chip is separately reduced and then combined with other exposures to improve signal. Bias and dark frames are subtracted from each raw image. Flat-fields are then traced and extracted for each fiber. Wavelength is calibrated using the arc lamp spectra and slightly adjusted to match the known positions of certain sky lines, which is then corrected to heliocentric frame. Further, the LAMOST one-dimensional (1D) pipeline extract and classify spectra into 4 categories (*star*, *galaxy*, *QSO* and *unknown*) where radial velocities, redshifts and other stellar parameters are calculated wherever possible (Zhao et al. 2012; Cui et al. 2012).

From 8,183,160 spectra classified as ‘*star*’ in LAMOST DR5, we selected 451,695 spectra belonging to O, B and A spectral type as given by LAMOST pipeline. LAMOST spectra with low Signal-to-Noise Ratio (SNR) may affect the selection and analysis of $H\alpha$ emission lines. In a study of identifying $H\alpha$ emission spectra from LAMOST DR2 by Hou et al. (2016), spectra with SNR of SDSS r band less than 10 ($SNR_r < 10$) were removed. Further, the automated routine to find emission lines in LAMOST spectra does not yield good accuracy if we reduce SNR $_r$ band less than 10 ($SNR_r < 10$). We observed that many noise peaks were reported as emission peaks. Hence, we adopted the criterion of $SNR_r > 10$ in order to remove the noisy spectra from our sample.

The reduced and calibrated spectra were downloaded from LAMOST DR5 website¹. The data array of a LAMOST fits file is as follows. The first frame contains the flux information, and the second frame contains the ‘inverse variance’ ($1/\sigma^2$, where σ is the uncertainty). The third frame stores wavelength in Å where as fourth and fifth frames contain ‘andmask’ and ‘ormask’ data. Further information about the fits description and data structure is accessible online². To normalize the spectra, we used `laspec`, a LAMOST spectral kit developed by Bo Zhang (Zhang et al. 2020). This python-based package is open-source and available in GitHub³. The entire spectrum is first smoothed using a smoothing spline and the pixels lying away from the 1.5σ threshold is removed. The remaining pixels are smoothed to obtain the pseudo-continuum, which is then used to obtain normalized spectrum. Refer to Section 2.1 of Zhang et al. (2020) for a detailed explanation regarding pre-processing of LAMOST spectra.

3 ANALYSIS

3.1 Identification of Emission-Line Stars from LAMOST DR5

In this section, we explain the method to identify the ELS with $H\alpha$ in emission in the Galaxy from the large data-set of LAMOST DR5. For the purpose of identifying ELS with $H\alpha$ in emission, we developed a python code based on `find_peaks` module in `scipy.signal` package (Virtanen et al. 2020). The important parameter in `scipy.signal.find_peaks` is “Width”, which corresponds to the full width at half maximum (FWHM) of the emission profile. Spikes in the spectrum caused by instrumental defects will be very narrow and can be mistaken for a narrow emission line. To remove such lines, we used a width cutoff of 3 sampling points. This reduces the possibility of false emission (caused by instrumental defects or noise) near $H\alpha$ being reported as real emission in the spectrum. We consider $H\alpha$ emission to be true only if Full Width at Half Maximum (FWHM) is at least 3 sampling points wide. Even though it affects the completeness of ELS from DR5, probability of reporting false emission is reduced compared to selection criteria used in Hou et al. (2016). The scope of this work is to provide a comprehensive catalog of stars with $H\alpha$ in emission which justifies the use of our stringent selection criteria. Out of 451,695 O, B, and A spectra from LAMOST DR5, we identified 5,437 spectra with $H\alpha$ in emission. Through a visual check, those without any photospheric features and broken spectra were removed, resulting in 4138 good quality spectra with $H\alpha$ in emission from LAMOST DR5. The selection scheme and the classification procedure we followed to identify 4138 emission-line spectra from LAMOST DR5 is represented in the form of a flowchart in Figure 2. It should be noted that if FWHM criterion is relaxed to a lower value, say to 1 sampling point, the number of ELS found would increase drastically but it may consist of many false detections.

From Figure 1, it can be seen that most of the ELS belong to the Galactic anti-centre direction while a few objects are within $60^\circ \leq l \leq 90^\circ$. Yuan et al. (2015) reported that the LAMOST Spectroscopic Survey of the Galactic Anti-centre (LSS-GAC) survey initially aimed to observe the Galactic thin/thick disks and halo for a contiguous sky area which is centred on the Galactic anti-centre direction ($150^\circ \leq l \leq 210^\circ$). Also, for large

¹ dr5.lamost.org

² http://dr5.lamost.org/v3/doc/data-production-description

³ https://github.com/hypergravity/laspec

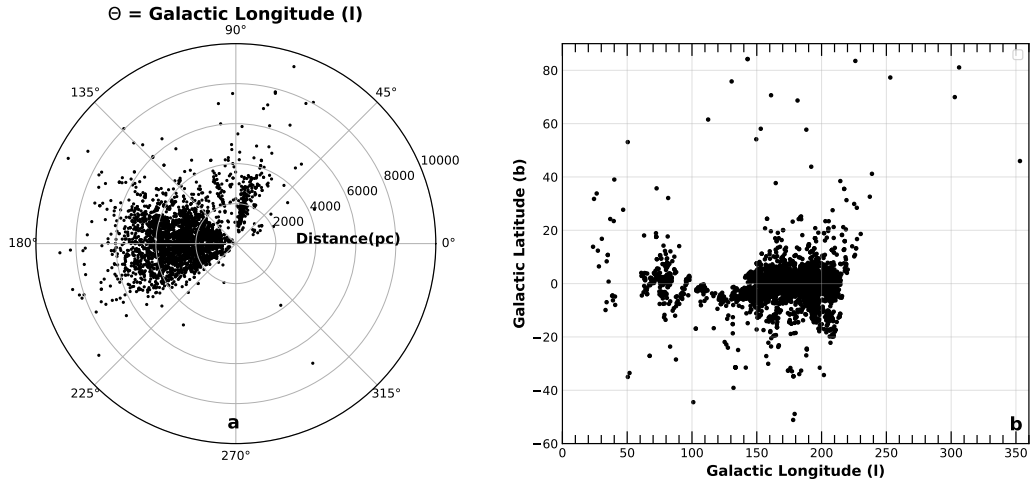


Fig. 1: The polar and spatial distribution of 3339 ELS in the Galaxy identified from LAMOST DR5 is shown. Fig 1a (left) shows the polar distribution of ELS in the Galactic Longitude (l) vs Distance (d) plane. Distances are taken from [Bailer-Jones et al. \(2021\)](#). The ELS are concentrated in the Galactic anti-center direction due to the observational strategy adopted by LAMOST ([Hou et al. 2016](#)). Fig 1b (right) represents the spatial distribution of ELS in Galactic Latitude (b) vs Galactic Longitude (l) plane. It can be seen that most of the ELS are found to be within $150^\circ \leq l \leq 200^\circ$ and $|b| \leq 20^\circ$.

distances, the inverse relation between *Gaia* EDR3 ([Lindgren et al. 2021](#)) parallax and distance fails. This was resolved by [Bailer-Jones et al. \(2021\)](#) using a probabilistic approach to determine the distance from *Gaia* EDR3 parallax. The distance range observed here shows that the sample of ELS observed is spread over 10 kpc with about 90% of the objects within 5.5 kpc. 53 objects are present in the high galactic latitude region ($|b| \geq 40^\circ$) which may be of further interest to readers, but is out of scope of this work.

3.2 Spectral Type Re-estimation

The spectral type of each LAMOST DR5 spectrum is estimated using LAMOST stellar parameter pipeline (LASP; [Wu et al. 2011](#)). The raw CCD images are processed through the 2-dimensional (2D) reduction pipeline ([Cui et al. 2012](#)) and the output is in the form of 1-dimensional (1D) spectrum for each star. The spectral type of the star is estimated through template matching with standard spectral templates and line recognition algorithms ([Luo et al. 2015](#)). A sample of 183 stellar spectra from LAMOST pilot survey and LAMOST DR1 were selected as standard spectral templates ([Wei et al. 2014; Kong et al. 2019](#)). For classifying O and B type stars, LAMOST pipeline has used only O, B, B6, and B9 stellar templates. The presence of the veiled continuum and emission lines formed outside the photosphere complicate the spectral classification in early-type stars ([Hernández et al. 2004](#)). For this reason, automated spectral type estimation for ELS may give erratic results. This was validated by our finding that, despite eliminating bad spectra from our sample, spectra classified as A-type by LASP show HeI absorption lines. Hence we need to re-estimate the spectral types for all the spectra. Thus, one has to resort back to semi-automated template matching technique where the user needs to select the best fit considering various spectral lines. In order to distinguish O, B and A type spectra, we can use the profile of Balmer absorption lines. Since we are dealing with emission-line spectra, we cannot use $H\alpha$, $H\beta$ and even $H\gamma$ to some extent because the emission mechanism can fill in these absorption lines. Hence as a first check, we matched the $H\delta$ and $H\epsilon$ profiles to estimate the spectral type coarsely. To estimate the spectral sub-class, we used absorption lines such as HeII, HeI and Mg II. Theoretically, one expects ionized HeII lines in O-type stars. The HeII lines fade as we move towards B-type stars where HeI absorption lines are stronger and further HeI lines slowly disappear in early A-type stars ([Gray & Corbally 2009](#)). Also, since CBe stars are fast rotators ($200\text{-}300 \text{ km s}^{-1}$), the depth or profile shape vary depending on the $v \sin i$ parameter. This will in turn affect the spectral type re-estimation process if we focus on the depth of lines ([Slettebak et al. 1980](#)). Keeping this in mind, we matched the wing profile of $H\epsilon$, $H\delta$, HeI and MgII lines rather than the depth of the line. However, estimating accurate spectral type for CBe stars using low-resolution spectra is difficult and one can expect up to an error of 2 sub-classes in B-type stars. To see the comparison between LAMOST candidate spectra and MILES template spectra, please refer to Figure 2 of [Anusha et al. \(2021\)](#).

As explained above, we performed spectral type re-estimation using semi-automated template matching method. For this, we used the MILES stellar spectral library ([Sánchez-Blázquez et al. 2006](#)) since it has sim-

ilar resolution ($R \sim 2000$) to LAMOST DR5 spectra ($R \sim 1800$). The homogeneously calibrated 985 spectra in MILES spectral library were obtained from the 2.5 m Isaac Newton Telescope (INT), covering a range of 3525–7500 Å (Falcón-Barroso et al. 2011). The template stars cover a wide parametric space, i.e. $T_{eff} = 3000 - 40,000$ K, $\log(g) = 0.2 - 5.5$. Out of 985 MILES templates, 79 of them are in the spectral range B0 – A9 covering luminosity classes III – V. Rest-frame correction to LAMOST DR5 spectrum were made using the redshift value provided by LASP. We developed a python code, which for a given spectra identifies 3 best-fitting templates (based on the chi-square value. Lower the chisquare value, better the fit) after iterating over the entire MILES library. To make sure the HeI and MgII absorption lines fit well, we over-plotted each spectra with top 3 template matches and visually identified the best among them. In most cases, the least chi-square valued template fitted the best to the spectra, but in a few cases, second or third least chi-square valued template fitted the higher-order Balmer lines ($H\delta$ and $H\epsilon$), HeI 4471 Å and MgII 4481 Å lines better, which justifies the time-intensive spectral typing procedure. Out of 4138 ELS spectra, we were able to ascertain spectral types to 3307 spectra. At this stage, spectra showing nebular forbidden lines such as [NII], [SII] and [OI] were identified using an automated python routine, which is explained in Appendix B. These spectra are classified as either A[em] or B[em]⁴ based on re-estimated spectral types. We could not assign a spectral type to 831 spectra because the blue end of the spectra were noisy and they are classified as “Em” or “Em[em]” (if forbidden lines are present).

3.3 Evolved Star Candidates

The evolved and highly luminous stars (post-main sequence/supergiants) with early spectral type are reported to have $H\alpha$ in emission (Rosendhal 1973). The $H\alpha$ emission in evolved stars primarily originates from wind driven mass loss (Weymann 1963; Hutchings 1970). The individual reddening for each spectrum co-ordinate was obtained using the `dustmaps` open source package (Green 2018), which provides probabilistic reddening measurements based on *Gaia* parallax and stellar photometry from 2MASS and PanSTARRS 1. The reddening $E(g - r)$ obtained using `dustmaps` is converted to $E(B - V)$ applying a general correction of 0.884⁵. Using these reddening measurements, we calculated the extinction in the V band by applying the relation $A_V = 3.1 \times E(B - V)$. The extinction in photometric bands of *Gaia* and 2MASS is then determined by adopting the conversion relations from Wang & Chen (2019).

To identify evolved stars present in our sample, two methods, spectroscopic (first) & photometric (second), are used. First, 42 spectra with luminosity class Ia/b & II estimated using MILES library are classified as “Evolved*”⁶. In addition, there can be some evolved stars whose luminosity class is misclassified. Hence as a second criteria, we used bolometric luminosity (L_{bol}) limit adopted from Lamers et al. (1998). The criteria of $\log(L_{bol}/L_{\odot}) > 4.5$ applied to all the remaining stars. We used *Gaia* BP (G_{BP}) magnitude and performed necessary bolometric corrections to calculate $\log(L_{bol}/L_{\odot})$. The equation for bolometric magnitude using G_{BP} is given below,

$$M_{bol} = G_{BP} - 5\log(d) + 5 + BC - A_{G_{BP}} \quad (1)$$

where BC is the bolometric correction taken from Jordi et al. (2010) for the re-estimated spectral types. $A_{G_{BP}}$ is calculated using conversion co-efficient taken from Wang & Chen (2019), which is given as $A_{G_{BP}} = 1.002 \times A_V$. The (L_{bol}/L_{\odot}) is calculated using the following equation,

$$\frac{L_{bol}}{L_{\odot}} = \frac{L_o}{L_{\odot}} \times 10^{-0.4M_{bol}} \quad (2)$$

where L_o is the zero-point luminosity equals 3.0128×10^{28} W. Using the above equation, we classified 4 additional spectra as “Evolved*” as they satisfy the photometric criteria. In total, 46 spectra are classified as ‘Evolved*’, of which 26 spectra belong to B2 or earlier spectral type.

3.4 Estimation of IR excess in ELS

The spectral energy distribution (SED) of main-sequence and PMS ELS show excess flux over the blackbody distribution in the infrared. This is indicative of the presence of a circumstellar disk in ELS (Natta et al. 1993). Infrared continuum excess observed in CBe stars is due to thermal *bremstrahlung* emission from the circumstellar disk (Gehrz et al. 1974). For CBeAe, the excess is predominantly concentrated in the NIR region. For HAeBe stars, the IR excess is attributed due to the thermal emission from the dust in the accretion disk (Hillenbrand et al. 1992; Malfait et al. 1998).

In order to differentiate main-sequence ELS (CBeAe) and PMS stars (HAeBe), we used two proxies of IR excess. Firstly, we chose all the objects with Two Micron All-Sky Survey (2MASS; Cutri et al. 2003) magnitudes

⁴ It should be noted that [em] is used to denote spectra with forbidden lines instead of [e] because [e] stars are conventionally defined to have [FeII] lines (Swings 1973)

⁵ `argonaut.skymaps.info/usage`

⁶ “*” is used here to denote that they are Evolved star candidates, a convention we have used throughout this work.

satisfying the criteria that reddening corrected $(H - K_S)_0$ color is greater than 0.4, which is a well-established cut-off to select HAeBe stars (Finkenzeller & Mundt 1984). Secondly, we calculated two spectral indices (Lada 1987; Wilking 1989; Greene et al. 1994) from the SEDs as proxies to quantify NIR and mid-infrared (MIR) excess. NIR spectral index (n_{J-K_S}) is calculated using 2MASS J and K_S magnitudes and MIR spectral index (n_{K_S-W2}), with 2MASS K_S and Wide-field Infrared Survey Explorer (WISE; Cutri et al. 2014) $W2$ magnitudes. The equation defining the spectral index is calculated as given in Equation 3. λ_1 and λ_2 represent the wavelength of two bands for which spectral index is calculated. F_{λ_1} and F_{λ_2} represent the extinction corrected absolute flux measured at λ_1 and λ_2 .

$$n_{\lambda_1-\lambda_2} = \frac{\log\left(\frac{\lambda_2 F_{\lambda_2}}{\lambda_1 F_{\lambda_1}}\right)}{\log\left(\frac{\lambda_2}{\lambda_1}\right)} \quad (3)$$

Based on the availability of IR photometric values for 3339 unique objects, n_{J-K_S} was calculated for 2978 stars and n_{K_S-W2} index was calculated for 2743 stars. Figure 3 shows the classification of ELS based on n_{J-K_S} and n_{K_S-W2} . Remaining 597 stars did not have 2MASS or WISE magnitudes to calculate indices. We considered objects with $(n_{K_S-W2}) > -1.5$ to have MIR excess (Andre et al. 1993; Arun et al. 2019). In addition, we also segregated objects having $(n_{J-K_S}) > -1.5$ but $(n_{K_S-W2}) < -1.5$ into a separate class named ‘‘Ae/Be*-onlynir’’. These objects have excess in NIR but do not show excess in MIR wavelengths, which needs to be studied in detail.

3.5 Naming and Classification scheme

Even though we treated 4138 spectra as independent entities, many stars are observed multiple times during the 5-year observation cycle. Hence it is necessary to identify and name each spectra based on its observed coordinate. We sorted 4138 spectra based on its *snrr* value in descending order and assigned name of first (highest SNR) spectra as ‘‘LEMC 0001’’. LEMC is abbreviated as ‘‘LAMOST Emission-Line Catalog (LEMC)’’. If another spectrum has RA and DEC within $1''$ of ‘‘LEMC 0001’’, then new spectrum is named as ‘‘LEMC 0001_2’’ and the next observation of same object (if present) is named as ‘‘LEMC 0001_3’’, and so on. The same process is iterated over the entire list and spectra are named from LEMC 0001 to LEMC 3339.

Coming to the classification of 4138 spectra, we created various classes to accommodate the non-availability of photometry values in some cases. If a spectra classified as B-type does not have *Gaia* EDR3 or 2MASS photometry within search radius of $3''$, then it is classified as ‘‘Be**’’. Further if the same spectrum has *Gaia* EDR3 and 2MASS photometry but was not detected in WISE, we classified it as ‘‘Be**’’ since Lada spectral indices cannot be calculated. We classify a spectrum as ‘‘CBe’’ only if it satisfies all three conditions, i.e., $H\alpha$ in emission, $(H - K_S)_0 \leq 0.4$ and the criteria set by Lada indices. This makes our classification robust.

We noted that in a few cases the multi-epoch observations have conflicting classifications. For example, LEMC 265 has three observations until DR5 which are classified as HBe, HAe and Em in each case. This is because spectra classified as ‘‘Em’’ is noisy in the blue-end which made the spectral type estimation not possible. The spectral type of other two observations are estimated here to be B9 and A1V, which led to final classifications of HBe and HAe respectively. In another case, 7 multi-epoch observations of LEMC 0013 are classified into ‘‘CBe’’ (4 spectra) and ‘‘Evolved*’’ (3 spectra). Since the spectrum of LEMC 0013 with highest *snrr* values (LEMC 0013_1) is classified as ‘‘CBe’’, the star LEMC 0013 is put into list of 1089 unique CBe stars. Hence, care should be taken to select the best spectrum out of multiple observations.

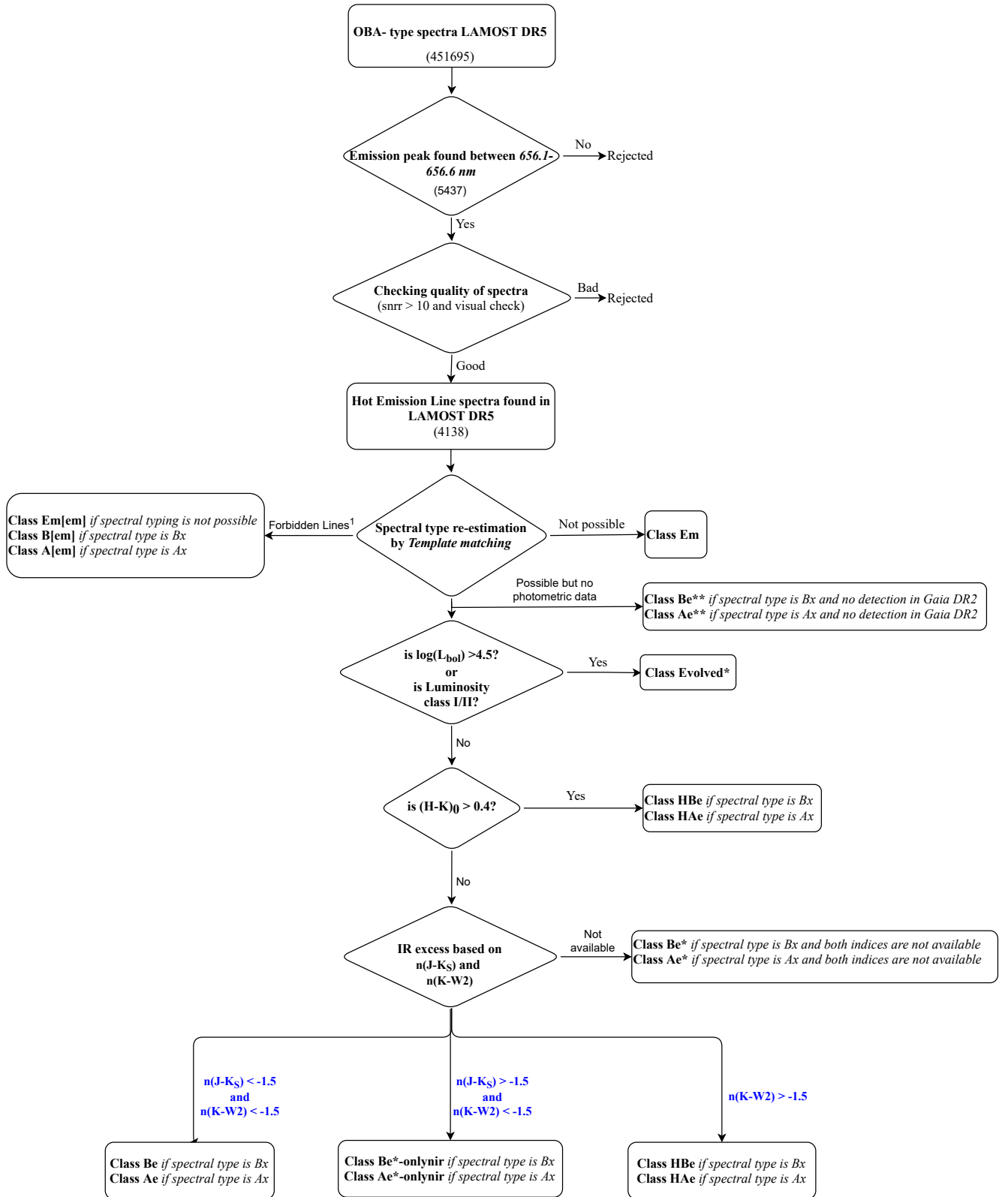
4 RESULTS

We classified 4138 spectra of 3339 unique ELS identified from LAMOST DR5 into various classes based on available Optical/IR photometry and presence of forbidden emission lines. Detailed classification algorithm is shown in form of a flowchart in Figure 2.

4.1 2MASS-WISE Color-Color Diagram

Presence of dust in the circumstellar environment/accretion disk of the ELS can be identified from the excess flux emission in the infrared wavelengths (Hartmann et al. 2005). We plotted the $(H - K_S)_0$ versus $(J - H)_0$ for CBe, CAe and HAeBe stars in Figure 4. As observed in the 2MASS CCDm (see Figure 4), CBe stars are more clustered together than CAe stars. Also, note that most of the HAeBe stars have $(H - K_S)_0 > 0.4$. It is seen that HAe stars strictly obey $(H - K_S)_0 > 0.4$ cutoff than HBe stars as suggested in Finkenzeller & Mundt (1984). IR excess in HBe stars is visibly evident in (n_{K_S-W2}) index than $(H - K_S)_0$ value.

Also, we have constructed a 2MASS-WISE CCDm where $(W1 - W2)_0$ is plotted against $(H - K_S)_0$ and is shown in Figure 4. Almost all HAeBe stars occupy a distinct region compared to CBeAe stars, which justifies our classification technique.



¹Forbidden lines considered here are [SII], [NII] and [OI](see Appendix 2 for details)

Fig. 2: The Classification procedure used in this work is explained as flowchart here. Various classes that are used in each step are explained in detail.

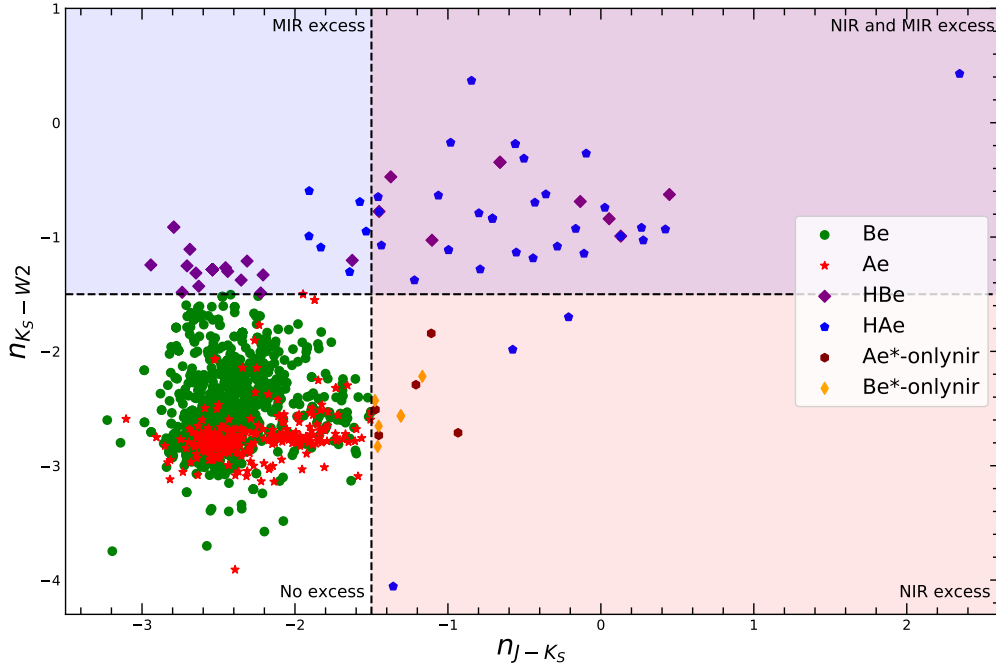


Fig. 3: The plot illustrates classification of different ELS into categories based on their NIR and MIR Lada indices (Lada 1987). The black dashed lines represent $(n_{J-K_S}) = -1.5$ and $(n_{K_S-W2}) = -1.5$. Classes such as Be (green filled circles), Ae (red filled stars), HBe (purple filled diamonds), H Ae (blue filled pentagons), Ae*-onlynir (brown filled hexagons), and Be*-onlynir (yellow solid thin diamonds) are shown in this figure.

Table 1: Statistics of classified spectra

Classification	Number of unique objects	Total number of spectra available	Classification	Number of unique objects	Total number of spectra available
CBe	1089	1523	CAe	233	286
H Ae	33	41	HBe	23	46
A[em]	605	637	B[em]	323	391
Em	196	307	Em[em]	490	524
Ae*	17	19	Be*	38	42
Ae**	17	18	Be**	168	182
Be*-onlynir	5	7	Ae*-onlynir	4	4
Evolved*	36	46	F[em]?	58	61
HFe?	1	1	Fe?*	3	3

4.2 Gaia Color-Magnitude Diagram

Gaia EDR3 provides G , G_{BP} and G_{RP} magnitudes for 3017 ELS present in our sample. The absolute G magnitude (M_G) is calculated using the distance values taken from Bailer-Jones et al. (2021). Further, the extinction corrected M_G and $(G_{BP} - G_{RP})_0$ color are plotted in Figure 5 for CBe, CAe and H AeBe stars. The Zero-age Main sequence (ZAMS) defined by Pecaut & Mamajek (2013) does not extend beyond B9 spectral type for M_G and $(G_{BP} - G_{RP})_0$ values. Hence we plotted the 60 Myr isochrone from the Modules for Experiments in Stellar Astrophysics (MESA) isochrones and evolutionary tracks (MIST⁷; Choi et al. 2016; Dotter 2016) in the *Gaia* CMD (Figure 5), which closely matches the ZAMS defined by Pecaut & Mamajek (2013). The MIST archive has provided isochrone corresponding to $(V/V_{crit} = 0.4)$ which is the only model available in the database for a rotating system. We adopted the metallicity $[Fe/H] = 0$ for the respective isochrone. It is clear that the CAe and CBe stars occupy overlapping regions whereas H Ae and HBe are well separated in *Gaia* CMD.

⁷ <http://waps.cfa.harvard.edu/MIST/>

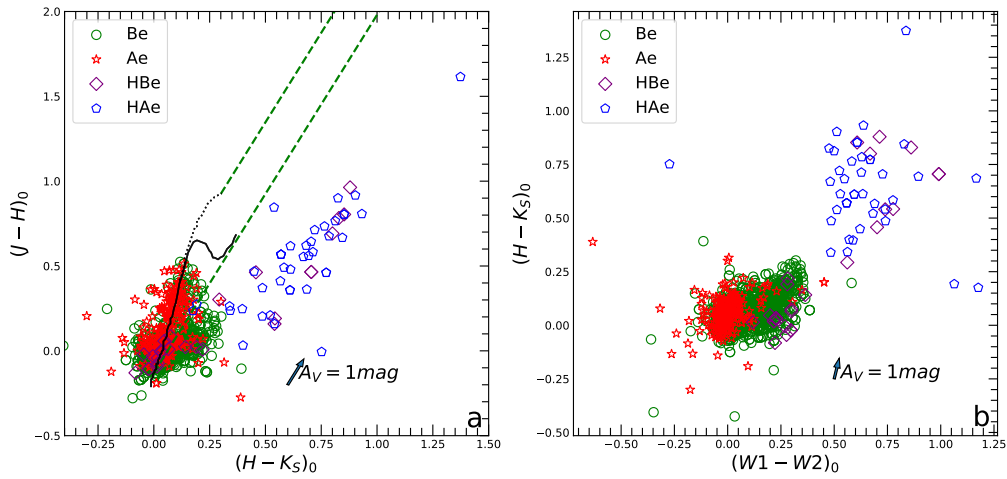


Fig. 4: (a). Reddening corrected 2MASS CCDm showing positions of CBe (green open circles), CAe (red open stars), HBe (crimson red open squares) and HAe (blue open pentagons) stars. (b) Reddening corrected 2MASS-WISE CCDm showing positions of CBe (green open circles), CAe (red open stars), HBe (crimson red open squares) and HAe (blue open pentagons) stars. The separation of main-sequence stars (CBe and CAe) from PMS stars (HBe and HAe) is very evident in the above plots. Arrow in both (a) and (b) represents the direction in which a star will move for an extinction of $A_V = 1$ mag.

4.3 Spectral Features of various classes

In this subsection, we discuss the spectral features present in the stars in various evolutionary phases, as identified in this work. A breakup of 3339 ELS identified is shown in Table 1.

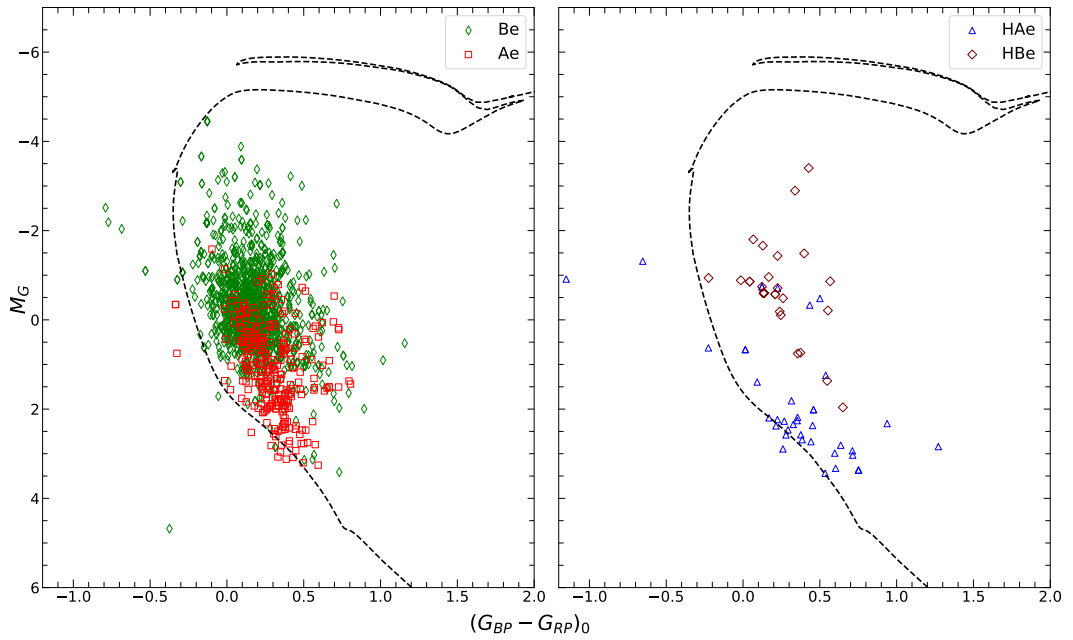


Fig. 5: *Gaia* CMD for CBeAe (left) and HAeBe stars (right) are shown. CBe (green open thin diamonds), CAe (red open squares), HBe (crimson red open diamonds) and HAe (blue open triangles) are shown. Dotted line in both the panels represents the isochrone of 60 Myr plotted in the *Gaia* CMD with $(V/V_{crit} = 0.4)$ and $[Fe/H] = 0$.

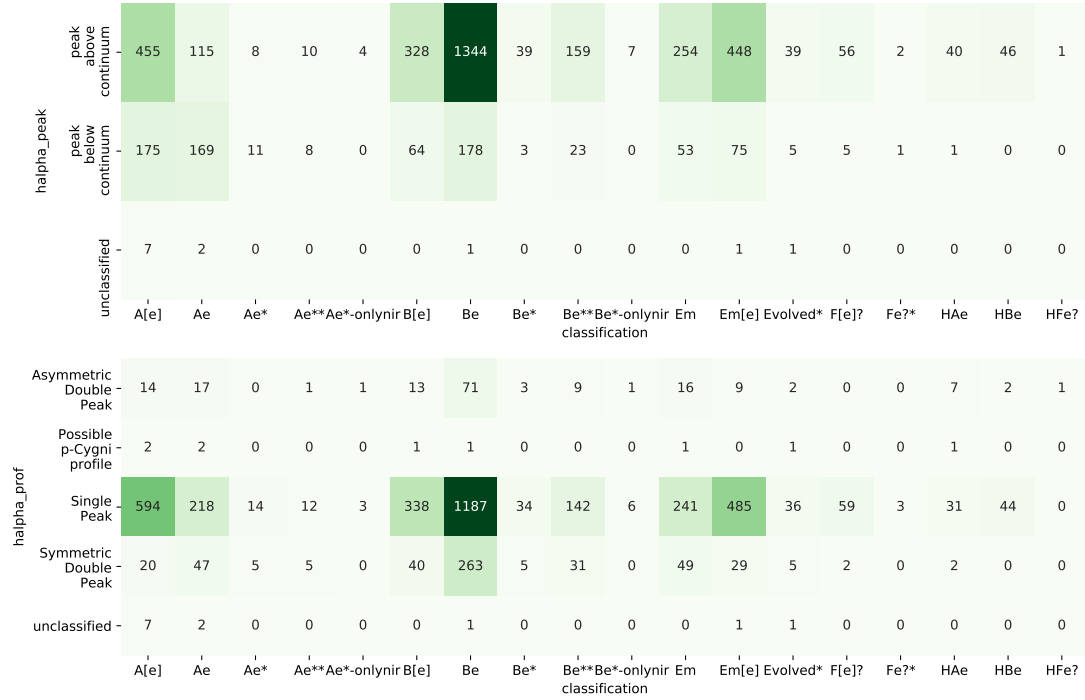


Fig. 6: (top) A heatmap representing the statistical distribution of spectra based on classification of identified ELS spectra and position of H α peak in the spectra. (bottom) A heatmap representing the statistical distribution of spectra based on classification of identified ELS spectra and the morphology of H α peak in the spectra. The number of spectra belonging to each class is shown inside the respective boxes.

4.3.1 Morphology of H α

In addition to classification of spectra explained in Section 3, we visually examined the spectra and noted different morphologies of H α emission seen in our sample. Out of 4138 ELS spectra identified in this work, 81% of the spectra show strong emission with the H α peak above the continuum and remaining 19% show weaker emission where the H α peak is seen inside the absorption core (emission-in-absorption). Further, 83% of the spectra show single peak profile, 12% show a symmetric double peak emission profile and 4% show an asymmetric double peak emission profile. Statistical breakup of 4138 spectra based on H α profile morphology, H α peak and classification is shown in Figure 6 as a heatmap.

4.3.2 Classical Be stars

We identified a homogeneous sample of 1523 spectra belonging to 1089 CBe stars in this study. In addition to the photospheric absorption lines, the spectra of CBe stars generally show emission lines of different elements such as hydrogen, helium, oxygen, iron, calcium, etc. A detailed examination of these lines help us understand the properties of the gaseous disk.

As mentioned in previous literature (Banerjee et al. 2021; Rivinius et al. 2013; Saad et al. 2012; Mathew & Subramaniam 2011), our sample of CBe stars also show diverse profiles in the Balmer lines. About 88% of spectra classified as CBe show H α in central emission above continuum and 12% show emission-in-absorption. 78% of spectra show single peak emission and 22% of the spectra show double peak emission. Around 45% of the spectra show H β in weak emission-in-absorption. All of our sample stars show H γ and higher-order Balmer lines in absorption. Interestingly, we also observe variability in line profiles/intensity in some cases. Apart from hydrogen, we observe that few CBe stars in our sample also show OI and FeII lines in emission. Studies on the emission line features of FeII lines is sparse in literature when compared to H α , due to the fact that FeII lines are difficult to detect. Additionally, a closer view on the variability of FeII lines compared to Balmer lines provide immense aid in understanding the kinematics of Be star disks. A dedicated analysis on these major line features observed in CBe stars will be presented as a follow-up work in Anusha et al. (in prep).

4.3.3 Classical Ae stars

We classified 286 spectra as CAe in this work with 169 spectra showing emission-in-absorption profile and 115 spectra showing emission above continuum. Since A-type stars have the strongest Balmer absorption lines, we observe more spectra with $H\alpha$ emission peak below the continuum. 76% of the CAe spectra show single-peak emission, 16% show symmetric double-peak emission and only 6% show asymmetric double-peak emission.

Out of 233 unique CAe stars identified, 159 CAe stars were analysed in detail by [Anusha et al. \(2021\)](#). The mismatch in number of CAe stars reported in their work and in our sample is due to a more stringent criteria of considering $V-[12]$ magnitude color excess, where [12] is the IRAS 12 μm magnitude from IRAS Point Source catalogue and V queried from APASS. The CAe stars are expected to show weak $H\alpha$ emission compared to CBe stars ([Rivinius et al. 2013](#)). For the sample of 159 CAe stars, they observed that $H\alpha$ EWs corrected for the underlying photospheric absorption are within the range of -0.2 to -23.6 \AA , which is comparatively lower than that reported for CBe stars. They also identified other emission lines such as FeII, OI, CaII triplet and Paschen series in hydrogen lines from their sample of CAe stars.

4.3.4 HAeBe stars

We identified 87 spectra belonging to 56 HAeBe stars in this work. 86 out of 87 spectra show $H\alpha$ emission above the continuum. 87% of HAeBe spectra show single-peak emission, 10% show asymmetric double-peak emission and less than 2% show symmetric double peak emission. It is interesting to see that 10% of HAeBe show asymmetric double-peak emission whereas only 4% of CBeAe spectra show asymmetric double-peak emission.

Apart from the presence of Balmer lines, HAeBe stars share spectral similarities with those of CBeAe, which include OI lines, CaII infrared triplet and the Paschen series of HI ([Persson & McGregor 1985](#); [Hamann & Persson 1992](#)) are also seen in our sample of spectra. Other emission lines present in the spectra of HAeBe stars are CaII H and K lines, NaI, and MgII. Since, we have removed the spectra with nebular forbidden lines from the analysis, the sample of HAeBe stars is not complete. Nidhi et al. (in prep) will consider this caveat and present an analysis of a bigger sample of intermediate-mass HAeBe stars from LAMOST DR5 including F0-F5 spectral types.

4.4 SIMBAD crossmatch

Finally, the newly identified ELS are cross matched with the SIMBAD database. Out of 3339 unique ELS, 623 objects have a record in SIMBAD database, among which 174 objects are marked as “Em*” (Emission-line star) and 17 stars are recorded as “Be*” (Be star) or “Ae*” (Herbig Ae/Be star). 356 objects are represented as “*” (Star) with no specific classifications. 22 objects are recorded as “Y*O” (Young Stellar Object) or “Y*?” (Young Stellar Object Candidate) and 7 objects are given as “WD?” (White Dwarf candidate) by [Zhang et al. \(2013\)](#). Other types that are seen are “IR” (IR source), “Ir*” (Variable Star of irregular type), “V*” (Variable star), “Ro*” (Rotationally Variable star) and “HB*” (Horizontal Branch star). All of the objects marked in SIMBAD as “Be*” are classified by us as “Be” and objects marked as “Y*O” are classified either as “HAeBe” or “A[em]/B[em]”. Most of our classification is in accordance with what is reported in SIMBAD, the only notable differences are the 7 stars that are classified as “WD?” by [Zhang et al. \(2013\)](#). In short, through this work of identifying the ELS from LAMOST DR5, we report 2716 new ELS which do not have any record on SIMBAD database. Figure 7 shows a representative sample of spectrum from some of the classifications discussed in this work.

5 CONCLUSION

We provide a catalog of 3339 hot (O, B and A spectral type) ELS identified from LAMOST DR5, of which 2716 are newly reported. Using an automated python routine, we identified 5437 spectra with $H\alpha$ in emission and visually selected 4138 good quality spectra for further analysis. We noticed that the spectral type provided by LAMOST is not accurate, deviating a few sub-classes in some cases. It is possible that emission features of the spectra is the reason for such mis-classifications. We re-estimated the spectral type of 3307 O, B and A type spectra by a semi-automated python routine that identifies three best template fits to the spectra in blue region including higher-order balmer lines such as $H\delta$ and $H\epsilon$ and then the best fit of the three templates (giving more importance to HeI and MgII lines) was selected visually. Our re-estimated spectral type matches better with spectral type given in SIMBAD than spectral type provided by LASP, which validates our technique. Once the spectral types were re-estimated, we distinguished stars with excess in NIR and MIR bands based on 2MASS $(H - K_S)_0$, (n_{J-K_S}) , and (n_{K_S-W2}) values. IR excess in NIR and MIR colors indicates the presence of dust in the circumstellar disk of PMS stars. CBe stars show low excess in NIR whereas HAeBe stars show considerable excess in NIR and sometimes a large excess in MIR as seen in Figure 4. We categorized the $H\alpha$ profiles of all 4138 emission-line spectra visually and it is represented as heatmap with respect to each classification, shown in Figure 6.

We present in context a caveat associated with our classification. As explained in subsection 3.5, in some cases stars with multiple observations can end up having multiple classifications. This occurs due to the inability

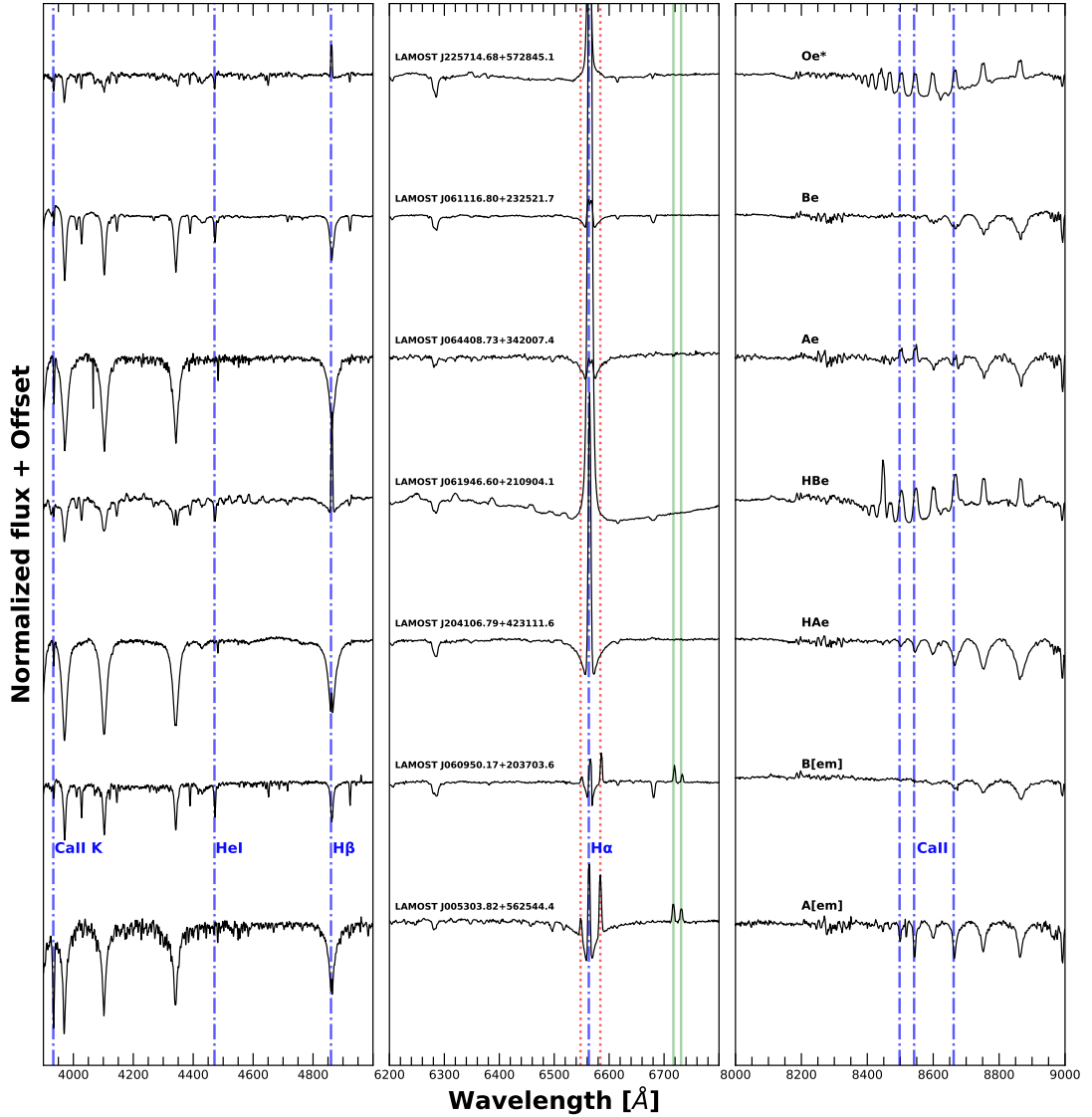


Fig. 7: This plot shows a representative spectrum belonging to each of Oe*, CBe, CAe, HBe, HAe, B[em], and A[em] classes. Red dotted lines denotes [NII] lines at 6548 and 6584 Å and green solid lines denotes [SII] lines at 6717 and 6731 Å. The spectra is normalized using `laspec` (Zhang et al. 2020) module.

of distinguishing B8/9 type from A0/1 type spectra owing to low-resolution of LAMOST DR5 spectra. LAMOST Mid-Resolution Spectra (MRS) in DR6/7 will be helpful to resolve this confusion.

In this work we report a homogeneous list of 1089 CBe, 233 CAe, 56 HAeBe stars, and 686 stars categorized as “Em” or “Em[em]”. In addition to these classes, we report 240 CBeAe candidates as “Be*/**” and “Ae*/**”. It may be noted that 159 CAe stars identified from this work is analyzed in detail in Anusha et al. (2021). We classified 928 objects either as “B[em]” or “A[em]” due to presence of [SII], [NII] and/or [OI] forbidden lines. Such a homogeneous list of emission-line catalog will help the community in studying ELS in detail without worrying about the bias associated with resolution and classification schemes when spectra is compiled from

various sources. A sample of identified ELS is shown in Appendix C and the entire catalog will be made available online in machine-readable format.

Acknowledgements We would like to thank the Science & Engineering Research Board (SERB), a statutory body of Department of Science & Technology (DST), Government of India, for funding our research under grant number CRG/2019/005380. We thank the Center for Research, CHRIST (Deemed to be University), Bangalore, India, for funding our research under the grant number MRP DSC-1932. We thank our colleagues Edwin Das and Robin Thomas for their valuable comments on the manuscript. This work has made use of data products from the Guo Shoujing Telescope (the Large Sky Area Multi-Object Fibre Spectroscopic Telescope, LAMOST). This work has made use of data from the European Space Agency (ESA) mission *Gaia* (<https://www.cosmos.esa.int/gaia>), processed by the *Gaia* Data Processing and Analysis Consortium (DPAC, <https://www.cosmos.esa.int/web/gaia/dpac/consortium>). Funding for the DPAC has been provided by national institutions, in particular the institutions participating in the *Gaia* Multilateral Agreement. We thank the SIMBAD database and the online VizieR library service for helping us in literature survey and obtaining relevant data.

Appendix A: CATALOG DESCRIPTION

Table A.1: Description of columns present in the catalog

Columns	Description
<i>specname</i>	Name of FITS file as given by LAMOST
<i>classification</i>	Class that the spectra belongs to
<i>catalog_name, unique_name</i>	Name assigned to the spectra in this work. <i>unique_name</i> gives the name of ELS star the spectra belongs. In addition to <i>unique_name</i> , <i>catalog_name</i> contains an extra number to identify spectra with highest <i>snrr</i> value. That is, if an ELS has multi-epoch spectra, then the highest <i>snrr</i> spectra will be denoted by “_1” in its <i>catalog_name</i>
<i>spectral_type</i>	Spectral type assigned to the spectra. The spectral type of best fit template from MILES library is provided.
<i>halpha_profile_comments</i>	Comments on H-alpha emission profile, visually checked
<i>forb_visual_comments</i>	Comments on forbidden lines present in spectra, visually checked
<i>l6300, l6363, l6548, l6584, l6717, l6731</i>	“yes” or “no”, based on an automated line finder routine. The code and threshold used is explained in Appendix 2.
<i>lamost_design_id</i>	The ID as provided in LAMOST DR5
<i>_RAJ2000, _DEJ2000</i>	Observed RA and Dec in degrees as given in FITS header
<i>subclass</i>	Spectral type assigned by LASP, as given in LAMOST DR5.
<i>snru, snrg, snrr, snri, snrz</i>	Signal-to-Noise Ratio of the spectrum in different SDSS bands, as given in LAMOST DR5.
<i>2MASS to Rfl</i>	2MASS photometry
<i>ALLWISE to qph</i>	ALLWISE photometry
<i>B - V to u.e.Bmag</i>	APASS photometry
<i>Av, Av.lower, Av.upper</i>	Extinction in V band queried from Green et al. (2019) . Upper and Lower bounds are given based on <i>r.low_photogeo</i> and <i>r.hi_photogeo</i> respectively
$n(J - K), n(K - W2)$	Lada indices calculated as defined in sect. 3.4
$(J - H)_0$ to $e_{-}(H - K)_0$	Extinction corrected 2MASS and WISE colors
<i>abs_Vmag</i> to $(B - V)_0$	Extinction corrected APASS absolute V magnitude along with errors and (B-V) color
<i>gaiaedr3_source_id</i> to <i>phot_rp_mean_mag_error</i>	<i>Gaia</i> EDR3 photometry
<i>r_med_geo</i> to <i>r_hi_photogeo</i>	Distances (geometric and photo-geometric) to the star along with upper and lower bounds based on <i>Gaia</i> EDR3 taken from Bailer-Jones et al. (2021) . “geometric” distance is calculated using parallax and a direction dependent distance prior, whereas “photo-geometric” used an additional color and apparent magnitude of the star.

Appendix B: FORBIDDEN LINES

To distinguish forbidden lines from noisy features in low-SNR spectra, we used the ‘prominence’ feature in ‘find_peaks’ module. We flagged a forbidden line as “yes” only if the prominence is greater than 0.2; if prominence value is between 0.1 and 0.2, it is flagged as “maybe” since it can be difficult to distinguish it from a noise feature if SNR is low and if prominence value is less than 0.1, the line is flagged as “no”. As CBeAe stars do not show forbidden lines such as [SII] $\lambda\lambda$ 6717,6731, [NII] $\lambda\lambda$ 6548,6584 and [OI] $\lambda\lambda$ 6300,6363 in their spectra, it is necessary to identify and remove spectra with above mentioned forbidden lines.

In addition to each forbidden line’s flag, the final decision was taken by visually selecting the spectra without any forbidden lines. We included the flags keeping in mind the future works, where one can use the flags given to select a subset of spectra with specific forbidden lines.

Appendix C: SAMPLE OF ELS IDENTIFIED

Table C.1: Details of sample of ELS identified in our work

lamost_design_id	_RAJ2000	_DEJ2000	classification	spectral_type	catalog_name
LAMOST J043018.87+071233.5	67.578651	7.209331	A[em]	A1V	LEMC 2910
LAMOST J043020.98+455603.2	67.58745	45.934232	Be	B8III	LEMC 0675
LAMOST J043023.15+550408.8	67.596482	55.069113	Be*-onlynir	B8III	LEMC 0495.1
LAMOST J043025.78+490355.8	67.607458	49.0655	Em		LEMC 2122
LAMOST J043030.15+533334.7	67.625642	53.559666	Be	B5V	LEMC 0493
LAMOST J043041.64+432544.5	67.673508	43.429055	Be	B5V	LEMC 1863
LAMOST J043058.53+373855.7	67.743908	37.64883	Evolved*	A2Ib/II	LEMC 0458.1

LAMOST J043104.88+520145.7	67.770358	52.029388	Em[em]		LEMC 1862
LAMOST J043111.79+322932.7	67.79914	32.492425	Be	B9III	LEMC 0896.1
LAMOST J043131.26+475750.7	67.880284	47.964108	Be	B2IIIvar	LEMC 0204.1
LAMOST J043133.92+523039.2	67.891338	52.510914	A[em]	A0III	LEMC 3203
LAMOST J043134.99+493650.1	67.895833	49.613944	Em		LEMC 2975
LAMOST J043153.91+430248.7	67.974655	43.046862	Be	B6IV	LEMC 2246
LAMOST J043220.04+513458.1	68.083504	51.582813	Ae	A1V	LEMC 2131
LAMOST J043226.98+343056.2	68.11243	34.515624	B[em]	B8V	LEMC 0701
LAMOST J043229.03+540352.2	68.120962	54.064511	Be	B8III-IV	LEMC 0408.1
LAMOST J043230.94+531036.0	68.128957	53.176687	Be	B5V	LEMC 1774.1
LAMOST J043244.07+554120.0	68.183645	55.688909	Be	B8	LEMC 0095.1
LAMOST J043247.86+455849.2	68.199448	45.980349	B[em]	B8V	LEMC 1947
LAMOST J043308.59+382811.8	68.285831	38.469964	Em[em]		LEMC 1628.1
LAMOST J043324.72+405849.1	68.353	40.980333	Be	B8	LEMC 1382.1
LAMOST J043327.11+512242.3	68.362983	51.37842	Be**	B8	LEMC 0020
LAMOST J043327.49+512242.4	68.364582	51.378454	Be**	B8	LEMC 0909
LAMOST J043347.36+330254.0	68.44737	33.048357	Em[em]		LEMC 2725
LAMOST J043431.86+442815.7	68.632762	44.471051	Be	B8V	LEMC 1205
LAMOST J043434.43+505322.9	68.643483	50.88972	Be	B9p+...	LEMC 1663.1
LAMOST J043434.61-025615.8	68.644226	-2.937746	Ae*	A1IV	LEMC 2382

References

- Akras S., Guzman-Ramirez L., Leal-Ferreira M. L., Ramos-Larios G., 2019, *ApJS*, **240**, 21
- Allen D. A., 1973, *MNRAS*, **161**, 145
- Andre P., Ward-Thompson D., Barsony M., 1993, *ApJ*, **406**, 122
- Anusha R., et al., 2021, *MNRAS*, **501**, 5927
- Arun R., Mathew B., Manoj P., Ujjwal K., Kartha S. S., Viswanath G., Narang M., Paul K. T., 2019, *AJ*, **157**, 159
- Bailer-Jones C. A. L., Rybizki J., Foesneau M., Demleitner M., Andrae R., 2021, *AJ*, **161**, 147
- Banerjee G., Mathew B., Paul K. T., Subramaniam A., Bhattacharyya S., Anusha R., 2021, *MNRAS*, **500**, 3926
- Barentsen G., et al., 2011, *MNRAS*, **415**, 103
- Choi J., Dotter A., Conroy C., Cantiello M., Paxton B., Johnson B. D., 2016, *ApJ*, **823**, 102
- Corradi R. L. M., et al., 2008, *A&A*, **480**, 409
- Corradi R. L. M., et al., 2010, *A&A*, **509**, A41
- Cui X.-Q., et al., 2012, *RAA*, **12**, 1197
- Cutri R. M., et al., 2003, *VizieR Online Data Catalog*, p. II/246
- Cutri R. e., et al., 2014, *VizieR Online Data Catalog*, pp II-328
- Deng L.-C., et al., 2012, *RAA*, **12**, 735
- Dotter A., 2016, *ApJS*, **222**, 8
- Drew J. E., et al., 2005, *MNRAS*, **362**, 753
- Drew J. E., et al., 2014, *Monthly Notices of the Royal Astronomical Society*, **440**, 2036
- Falc3n-Barroso J., S3nchez-Bl3zquez P., Vazdekis A., Ricciardelli E., Cardiel N., Cenarro A. J., Gorgas J., Peletier R. F., 2011, *A&A*, **532**, A95
- Finkenzeller U., Mundt R., 1984, *A&AS*, **55**, 109
- Gehrz R., Hackwell J., Jones T., 1974, *The Astrophysical Journal*, **191**, 675
- Gonz3lez-Solares E. A., et al., 2008, *Monthly Notices of the Royal Astronomical Society*, **388**, 89
- Gray R. O., Corbally Christopher J., 2009, *Stellar Spectral Classification*. Princeton university press
- Green G., 2018, *The Journal of Open Source Software*, **3**, 695
- Green G. M., Schlafly E., Zucker C., Speagle J. S., Finkbeiner D., 2019, *ApJ*, **887**, 93
- Greene T. P., Wilking B. A., Andre P., Young E. T., Lada C. J., 1994, *ApJ*, **434**, 614
- Hamann F., Persson S. E., 1992, *ApJS*, **82**, 285
- Hartmann L., Megeath S. T., Allen L., Luhman K., Calvet N., D'Alessio P., Franco-Hernandez R., Fazio G., 2005, *ApJ*, **629**, 881
- Herbig G. H., 1960, *ApJS*, **4**, 337
- Hern3ndez J., Calvet N., Brice3o C., Hartmann L., Berlind P., 2004, *AJ*, **127**, 1682
- Hillenbrand L. A., Strom S. E., Vrba F. J., Keene J., 1992, *ApJ*, **397**, 613
- Hou W., et al., 2016, *RAA*, **16**, 138
- Huang Y. F., Zeng Li J., Rector T. A., Mallamaci C. C., 2013, *AJ*, **145**, 126
- Hutchings J. B., 1970, *MNRAS*, **147**, 161
- Jaschek M., Egret D., 1982, in *Jaschek M., Groth H. G., eds, IAU Symposium Vol. 98, Be Stars*. p. 261

- Jaschek M., Jaschek C., Egret D., 1986, *Astronomy and Astrophysics*, 158, 325
- Jordi C., et al., 2010, *A&A*, 523, A48
- Joy A. H., 1945, *ApJ*, 102, 168
- Kalari V. M., et al., 2015, *MNRAS*, 453, 1026
- Kogure T., Leung K. C., 2007, *A Book on Astrophysics of Emission-Line Stars*. ASP, p. 260
- Kohoutek L., Wehmeyer R., 1999, *A&AS*, 134, 255
- Kong X., Luo A., et al., 2019, in *Astronomical Data Analysis Software and Systems XXVII*. p. 91
- Lada C. J., 1987, in Peimbert M., Jugaku J., eds, *IAU Symposium Vol. 115, Star Forming Regions*. pp 1–17
- Lamers H. J., Zickgraf F.-J., de Winter D., Houziaux L., Zorec J., 1998, *Astronomy and Astrophysics*, 340, 117
- Li G.-W., et al., 2018, *ApJ*, 863, 70
- Lin C.-C., Hou J.-L., Chen L., Shao Z.-Y., Zhong J., Yu P.-C., 2015, *RAA*, 15, 1325
- Lindgren L., et al., 2021, *A&A*, 649, A2
- Luo A.-L., et al., 2015, *RAA*, 15, 1095
- Malfait K., Bogaert E., Waelkens C., 1998, *A&A*, 331, 211
- Mathew B., Subramaniam A., 2011, arXiv preprint arXiv:1108.5850
- Mathew B., Subramaniam A., Bhatt B. C., 2008, *Monthly Notices of the Royal Astronomical Society*, 388, 1879
- Merrill P. W., Burwell C. G., 1949, *ApJ*, 110, 387
- Natta A., Prusti T., Krugel E., 1993, *A&A*, 275, 527
- Pecaut M. J., Mamajek E. E., 2013, *ApJS*, 208, 9
- Persson S. E., McGregor P. J., 1985, *AJ*, 90, 1860
- Pettersson B., Armond T., Reipurth B., 2014, *A&A*, 570, A30
- Porter J. M., Rivinius T., 2003, *PASP*, 115, 1153
- Raddi R., et al., 2013, *MNRAS*, 430, 2169
- Reipurth B., Pettersson B., Armond T., Bally J., Vaz L. P. R., 2004, *AJ*, 127, 1117
- Rivinius T., Carciofi A. C., Martayan C., 2013, *A&A Rev.*, 21, 69
- Rodríguez-Flores E. R., Corradi R. L. M., Mampaso A., García-Alvarez D., Munari U., Greimel R., Rubio-Díez M. M., Santander-García M., 2014, *A&A*, 567, A49
- Rosendhal J. D., 1973, *ApJ*, 186, 909
- Saad S., Hamdy M., Abolazm M., 2012, *NRIAG Journal of Astronomy and Geophysics*, 1, 97
- Sánchez-Blázquez P., et al., 2006, *MNRAS*, 371, 703
- Slettebak A., Kuzma T. J., Collins G. W. I., 1980, *ApJ*, 242, 171
- Stephenson C., Sanduleak N., 1977, *The Astrophysical Journal Supplement Series*, 33, 459
- Stoughton C., et al., 2002, *The Astronomical Journal*, 123, 485
- Swings J. P., 1973, *A&A*, 26, 443
- Vink J. S., Drew J. E., Steeghs D., Wright N. J., Martin E. L., Gänsicke B. T., Greimel R., Drake J., 2008, *Monthly Notices of the Royal Astronomical Society*, 387, 308
- Vioque M., Oudmaijer R. D., Schreiner M., Mendigutía I., Baines D., Mowlavi N., Pérez-Martínez R., 2020, *A&A*, 638, A21
- Virtanen P., et al., 2020, *Nature Methods*, 17, 261
- Wackerling L. R., 1970, *MNRAS*, 149, 405
- Wang S., Chen X., 2019, *ApJ*, 877, 116
- Wang S.-G., Su D.-Q., Chu Y.-Q., Cui X., Wang Y.-N., 1996, *Appl. Opt.*, 35, 5155
- Waters L. B. F. M., Waelkens C., 1998, *ARA&A*, 36, 233
- Wei M., Stover R. J., 1996, in *Solid State Sensor Arrays and CCD Cameras*. pp 226–232
- Wei P., et al., 2014, *The Astronomical Journal*, 147, 101
- Weymann R., 1963, *ARA&A*, 1, 97
- Wilking B. A., 1989, *PASP*, 101, 229
- Witham A. R., et al., 2007, *MNRAS*, 382, 1158
- Witham A. R., Knigge C., Drew J. E., Greimel R., Steeghs D., Gänsicke B. T., Groot P. J., Mampaso A., 2008, *MNRAS*, 384, 1277
- Wu Y., et al., 2011, *RAA*, 11, 924
- Yao Y., Liu C., Deng L., de Grijs R., Matsunaga N., 2017, *ApJS*, 232, 16
- Yuan H. B., et al., 2015, *MNRAS*, 448, 855
- Zhang Y.-Y., et al., 2013, *AJ*, 146, 34
- Zhang B., Liu C., Deng L.-C., 2020, *ApJS*, 246, 9
- Zhao G., Zhao Y.-H., Chu Y.-Q., Jing Y.-P., Deng L.-C., 2012, *RAA*, 12, 723
- Štefl S., Baade D., Rivinius T., Stahl O., Budovičová A., Kaufer A., Maintz M., 2003, *A&A*, 411, 167